Award Number: W81XWH-11-1-0676

TITLE: Model-Based, Noninvasive Monitoring of Intracranial Pressure

PRINCIPAL INVESTIGATOR: George Verghese

CONTRACTING ORGANIZATION: Massachusetts Institute of Technology
Cambridge, MA 02139

REPORT DATE: July 2013

TYPE OF REPORT: Final

PREPARED FOR: U.S. Army Medical Research and Materiel Command
Fort Detrick, Maryland 21702-5012

REPORT DOCUMENTATION PAGE

Form Approved
OMB No. 0704-0188

1. REPORT DATE	2. REPORT TYPE	3. DATES COVERED
July 2013	Final	16 September 2011 – 30 June 2013

4. TITLE AND SUBTITLE

Model-Based, Noninvasive Monitoring of Intracranial Pressure

5a. CONTRACT NUMBER

5b. GRANT NUMBER
W81XWH-11-1-0676

5c. PROGRAM ELEMENT NUMBER

6. AUTHOR(S)

George C. Verghese, Professor of Electrical and Biomedical Engineering, MIT

E-Mail: verghese@mit.edu

5d. PROJECT NUMBER

5e. TASK NUMBER

5f. WORK UNIT NUMBER

7. PERFORMING ORGANIZATION NAME(S) AND ADDRESS(ES)

Massachusetts Institute of Technology
Cambridge, MA 02139

8. PERFORMING ORGANIZATION REPORT NUMBER

9. SPONSORING / MONITORING AGENCY NAME(S) AND ADDRESS(ES)
U.S. Army Medical Research and Materiel Command
Fort Detrick, Maryland 21702-5012

10. SPONSOR/MONITOR'S ACRONYM(S)

11. SPONSOR/MONITOR'S REPORT NUMBER(S)

12. DISTRIBUTION / AVAILABILITY STATEMENT
Approved for Public Release; Distribution Unlimited

13. SUPPLEMENTARY NOTES

14. ABSTRACT
The project aims were (i) to further develop and validate a novel model-based approach to noninvasive, calibration-free determination of intracranial pressure (ICP) from quantities that are routinely measured in clinical settings, and (ii) to initiate the creation of a publicly available and growing reference database of physiological signals collected from brain injury patients. A physiologically based model relates ICP to simultaneously measured waveforms of arterial blood pressure (ABP), obtained via radial artery catheter or finger cuff, and cerebral blood flow velocity (CBFV) at a major cerebral artery, measured by transcranial Doppler (TCD), thus enabling ICP to be estimated. Our initial target population comprised subarachnoid hemorrhage patients in the neuro-ICU at our partner hospital, for whom ICP, ABP and CBFV are currently measured as the clinical standard of care. The project's major accomplishments include: assembling a suitable system for data collection in the neuro-ICU; specifying a careful data collection protocol; arranging for the collected data to be transferred to the publicly accessible MIMIC II database; converting our earlier batch-mode ICP estimation algorithms to run in real time; and, on 28 windows of data processed thus far, obtaining ICP estimates with mean bias -0.7 mmHg, standard deviation of error 4 mmHg, and root mean square error 3.9 mmHg. These results are twice as good as in our earlier validation studies.

15. SUBJECT TERMS
Intracranial pressure (ICP), noninvasive monitoring, cerebrovascular model, cerebral blood flow velocity, transcranial Doppler (TCD), subarachnoid hemorrhage (SAH), traumatic brain injury (TBI), cerebral perfusion pressure

16. SECURITY CLASSIFICATION OF:			17. LIMITATION OF ABSTRACT	18. NUMBER OF PAGES	19a. NAME OF RESPONSIBLE PERSON
a. REPORT	b. ABSTRACT	c. THIS PAGE			USAMRMC
U	U	U	UU	41	19b. TELEPHONE NUMBER *(include area code)*

Contents

Chapter 1

Introduction

Intracranial pressure (ICP) is the pressure of cerebrospinal fluid (CSF) in the cranial cavity, and is an important "cranial vital sign" to monitor in patients with — or suspected of having sustained — an injury to the brain. However, current ICP measurement modalities are quite invasive, requiring penetration of the skull and placing a sensor in the brain parenchyma or advancing a catheter to the intraventricular space. ICP measurement is therefore usually reserved for cases of severe injury only, and for situations where the required neurosurgical expertise is available, thus excluding a large proportion of patients whose diagnosis and treatment could benefit from ICP measurements. Furthermore, no front-line device currently exists for medics to assess, track, and manage ICP in theater or during transport to a fully equipped trauma-care center. An accurate method for noninvasive and continuous tracking of ICP will have tremendous and immediate value for early diagnosis and treatment of brain injury, titration of therapy, and monitoring of disease progression. There is accordingly a need for a thoroughly validated, noninvasive method to assess and track ICP (and therefore cerebral perfusion pressure), ideally continuously, robustly, in a patient-specific manner, and without the need for calibration. This project was directed at further development of the algorithms, associated hardware, and clinical data collection required for broader validation of a novel model-based approach we have developed for noninvasive ICP estimation, which holds promise of meeting these criteria.

Chapter 2

Background and Objectives

Our approach to patient-specific, noninvasive ICP (nICP) determination generates estimates of ICP on a beat-by-beat timescale, from time-synchronized arterial blood pressure (ABP) and cerebral blood flow velocity (CBFV) waveform measurements that can be obtained quite routinely. Our processing of these waveforms exploits a simplified dynamic model of cerebrovascular physiology that relates the measured signals to ICP [1, 2, 3]. Validation tests prior to the current project were carried out on archived data from traumatic brain injury (TBI) patients, recorded in the 1990's by collaborators in the UK [1, 3].

2.1 Relevant physiology

In the cerebral vasculature, the pressure surrounding the veins is ICP, which — even under normal physiological conditions — exceeds the downstream cerebral venous pressure. Since veins are thin-walled and cannot withstand negative transmural pressure, cerebral veins enter a so-called Starling resistor regime in which blood flow is driven by the difference between ABP and ICP, rather than between ABP and cerebral venous pressure [4]. This is the reason for the clinical definition of cerebral perfusion pressure (CPP) as the difference between mean ABP and ICP; it is CPP that drives cerebral blood flow (CBF). The dependence of CBF on ICP (via its dependence on CPP) leads to the expectation that ICP can be determined from measurements of CBF and ABP.

2.2 Model-based estimation

To relate ABP and CBF to ICP, we have developed a simplified, aggregated mechanistic model of the cerebrovascular space. Figure 2.2.1 shows successive abstractions of the relevant physiology, resulting in the circuit analog in Figure 2.2.1C that is a convenient model for describing the ICP estimation process. Though the CBF shown in Figure 2.2.1B could represent the aggregate arterial inflow into the cerebral vasculature, for our purposes it denotes the flow in a major cerebral artery — the right or left middle cerebral artery (MCA), for example. The physical properties of the distributed vasculature are represented in Figure 2.2.1C by a single compliance element C that captures the aggregate compliance of the cerebral arteries and surrounding brain tissue, as seen from the MCA, and a single lumped resistive element R that represents the aggregate cerebrovascular resistance, again as seen from the MCA. These two lumped physical properties manifest themselves in the waveforms of cerebral ABP [p(t)] and CBF [q(t)]. The differential equation that governs the circuit model in Figure 2.2.1C supplies the dynamic constraint linking ABP and CBF to C, R, and ICP, and enables the latter three quantities to be estimated from measurements of the first two quantities [1].

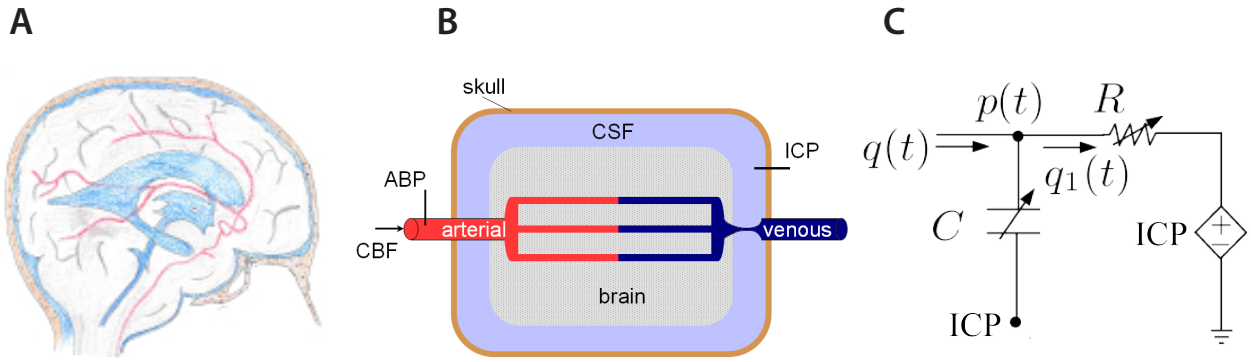

Figure 2.2.1: Progressive abstraction of cerebrovascular physiology. A: Relevant cerebrovascular anatomy; B: schematic representation of the main cerebrovascular compartments; and C: lumped circuit-model representation of cerebrovascular physiology, in which ICP denotes both extra-luminal pressure and effective downstream pressure.

2.3 Clinical measurements

Measuring CBF and ABP waveforms at the MCA (or any other major cerebral vessel) is not feasible. Rather, we obtain CBFV at the MCA (measured noninvasively using transcranial Doppler ultrasound, TCD) and ABP at a peripheral location (measured minimally invasively from the radial artery, though extension to noninvasive finger-cuff measurements is being planned), with careful time-synchronization of the two waveforms.

The use of CBFV rather than volumetric CBF affects our estimation of R and C, in that we can only estimate scaled versions of these parameters, where the scale factor is the unknown constant that is assumed to relate CBFV to CBF. However, absolute ICP can still be determined, as long as the CBFV–to–CBF scale factor remains essentially constant over the duration of an estimation window (typically comprising 30 to 60 heartbeats); the scale factor is allowed to vary from one window to the next. Under this assumption, the estimate of ICP is largely independent of the insonation angle of the cerebral vessel.

The measured ABP waveform at the radial artery or finger is undoubtedly different from the ABP measurement that would be obtained at the site of the CBFV measurement. Currently, we ignore differences in the morphology of these two waveforms, though we make a crucial time adjustment to compensate for the different effective path length from the heart to radial artery or finger, relative to the effective path length from the heart to the MCA [1].

To support the validation effort, invasive ICP and other routinely monitored data and patient information are also collected.

2.4 Estimation algorithm

By using our model in a coupled analysis of the detailed features of the CBFV and ABP waveforms, we develop an estimation algorithm that can compute the time adjustment or offset required to compensate for the differential path length mentioned above, and then sequentially estimate C, R, and ICP for each cardiac cycle, in a patient-specific manner, i.e., without the need for training on individual subject or population data. To mitigate the effects of noise and thus provide robust estimates, the algorithm actually computes the estimates via least-squared-error averaging over

windows comprising multiple consecutive beats of the input waveforms.

2.5 Project objectives

The current project was aimed primarily at further validation and improvement of the method, using data collected in a more carefully controlled and documented setting, using modern equipment, and on a different cross section of patients in neurocritical care. Our patients were those with subarachnoid hemorrhage (SAH), for whom CBFV measurement as well as invasive ICP measurement — which we need for our validation purposes — are clinically indicated. We aimed to record under data collection protocols that we would help standardize, and under circumstances that we could record in detail. The data we collect was intended to be made available for worldwide research use. We also aimed to move towards real-time estimation.

More specifically, our aims were to accomplish the following by the end of the project:

1. Develop a high-resolution data-acquisition infrastructure at the Neurological Intensive Care Unit (neuro-ICU) at Boston's Beth Israel Deaconess Medical Center (BIDMC), for time-locked collection of standard bedside monitoring data along with continuous CBFV signals and invasively measured ICP recordings.

2. Establish a framework for archiving continuous monitoring data and relevant clinical information from patients with critical brain injuries, to facilitate collection during and beyond this project, and to allow the resulting de-identified database to be made available on an on-going basis to the interested research community.

3. Seed the database with 30 patient records containing monitoring data and clinical information from the entire neuro-ICU stay of SAH patients admitted to the BIDMC during the project.

4. Validate our noninvasive ICP estimates against this initial database of brain-injury patients, and determine whether — with the instrumentation and data collection protocols now under our control — the performance metrics of our estimates improve over those demonstrated in our prior work, yielding ICP estimates that lie within clinically acceptable tolerances.

5. Demonstrate real-time performance of the validated noninvasive ICP estimation algorithm.

Chapter 3

Data Collection

To support refinement and validation of our noninvasive approach to ICP monitoring, we have established a data-acquisition infrastructure in the neuro-ICU at BIDMC that allows us to collect ICP, ABP, and CBFV waveforms during routine, clinically indicated TCD examinations of patients with subarachnoid hemorrhages. Additionally, we are able to capture all clinical information associated with the patient's stay in the neurocritical care unit, and the relevant bedside monitoring data, through the existing data-archiving infrastructure of the Multiparameter Intelligent Monitoring in Intensive Care II (MIMIC II) database [5]. Below, we describe the data collection process.

3.1 Acquisition of bedside monitoring data

To support our data acquisition, two key budgeted pieces of equipment were purchased during the first months of the project, namely the Component Neuromonitoring System (CNS, Moberg Research, Inc.) and the Spencer Technologies ST3 TCD System. Both instruments are FDA-approved medical devices. Their roles in our noninvasive ICP (nICP) estimation configuration are shown in Figure 3.1.1. The CNS device connects to both the Spencer TCD system and the Philips bedside monitor, and collects data in a time-synchronized manner from both devices. Additionally, the CNS monitor can be configured to accept important clinical information, such as Glasgow Coma Scale score, hematocrit, and patient age and gender.

We arranged and completed a TCD training session at BIDMC with an expert ultrasonographer

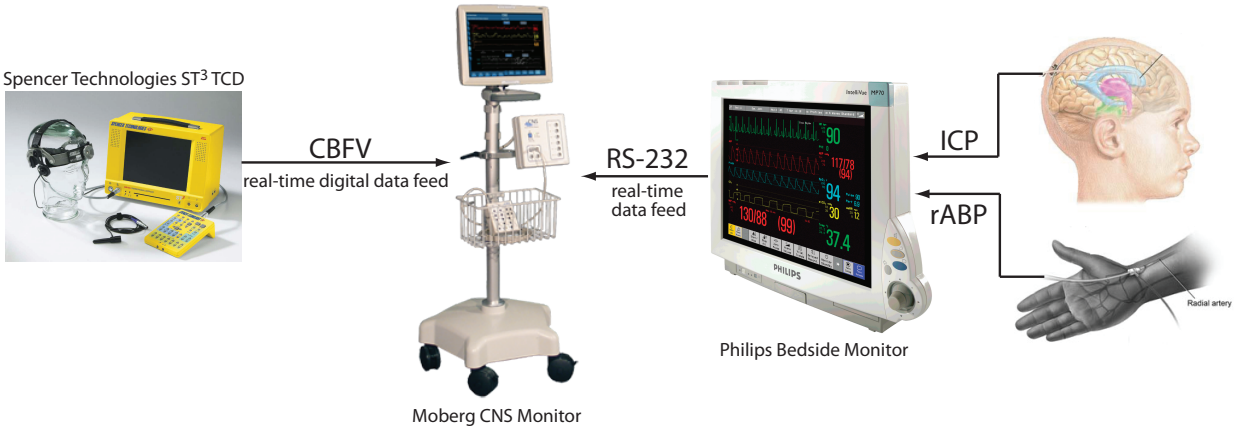

Figure 3.1.1: Data-collection infrastructure in the neurocritical care unit to support the data collection under this research project.

to understand the proper operation of the Spencer TCD device and also understand how a transcranial ultrasound examination is performed. Working with the biomedical engineering staff at BIDMC, we transitioned the CNS and TCD monitors into the neurocritical care environment. We have worked closely with the stroke neurologists at BIDMC who are conducting the TCD recordings on the target patient population.

In the BIDMC neurocritical care unit, the ABP waveform is uniformly measured with an indwelling radial artery catheter. In our SAH patients, the ICP signal is measured with a ventricular catheter placed into the anterior horn of a lateral ventricle. The catheter is connected to a pressure transducer and a ventriculostomy drainage bag that allows for CSF to be drained. The CBFV waveforms that are archived as part of this research project were collected during routine, clinically indicated TCD examinations for detection of vasospasm. During the TCD exam, the stroke neurologists generally insonate the middle, anterior, and posterior cerebral arteries of one hemisphere before examining the same vessels on the other hemisphere. The basilar artery, internal carotids, and ophthalmic arteries are subsequently examined.

3.2 Clinical information

In addition to the ABP, CBFV and ICP waveform data, the neurologists collect important clinical information during each recording session. The recorded information includes static patient demographics (age and gender) and dynamic clinical information, such as hematocrit and the Glasgow Coma Scale (GCS). Additionally, the clinical team records the vertical height (from the floor) of the ABP and ICP pressure transducers to estimate the hydrostatic pressure difference in ABP between the location of the ABP measurement and the location of the ICP measurement.

While the ICP estimation algorithm requires ABP calibrated to the level of the cerebral vasculature, the ABP measurement in critical care is commonly referenced to the level of the right atrium. The ABP calibration to heart level does not constitute a problem if the patient is in the supine position. In this case, mean ABP is approximately the same throughout the arterial system. However, most neurocritical care patients are placed in the head-up position to relieve intracranial congestion. In this case, the ABP that would be measured at the level of the cerebral vasculature is lower than the ABP at heart level, due to the hydrostatic pressure component that separates the two anatomical locations. By measuring the vertical distance from the ABP transducer to the ICP transducer, we can compensate in a post-processing step for this hydrostatic pressure difference, and thereby estimate the ABP that would have been measured at the level of the cerebral vasculature.

3.3 Device testing

We tested the TCD system and verified the data streaming capability. Furthermore, we tested the acquisition of CBFV data from both a unilateral probe, and a pair of bilateral probes affixed to a head frame. The data collected from the bilateral probes were remarkably stable with respect to even substantial head movement. While this was very encouraging for our purposes, the head frame was not usable in the neurocritical care setting, as it interfered with the positioning of other probes, most notably the ICP catheter.

In conjunction with the technical support staff at Spencer Technologies, we determined that the signal delay of the CBFV waveform envelope is on the order of 10ms (8ms of data accumulation

followed by FFT computation and other overhead). Feeding the CBFV signals from the Spencer TCD to the CNS system introduces further delays that can be in excess of 200ms because of the digital, packet-based data communication protocol. Delays of this magnitude can be very problematic for our ICP estimation algorithm if uncompensated, as they might lead to a lack of association of the CBFV wavelet to the corresponding ABP wavelet. We have therefore developed a data pre-processing step that assures the correct association of each CBFV wavelet with the corresponding ABP wavelet (see Chapter 5).

In our laboratory setting, we have explored a variety of possible interface options for the Spencer TCD, including digital data streaming via a USB port or using the analog output of the TCD machine, for both offline and real-time processing of the (unilateral or bilateral) CBFV signal. The analog output is suited to real-time processing. The digital data stream is suitable for feeding into the CNS, but currently not for real-time processing. Data stored on the Spencer TCD can also be used for offline processing. We have explored both real-time ICP estimation and off-line batch processing of the archived data. These explorations are detailed in Chapter 5.

Chapter 4

Database

4.1 The MIMIC II Database

To start our data collection, we first obtained MIT IRB and DoD HRPO approval for use of the data in the Multiparameter Intelligent Monitoring in Critical Care II (MIMIC II) database (http://mimic.physionet.org). The database is described more fully in [5]. This is an open-access, comprehensive clinical database to support work towards next-generation ICU patient-monitoring systems. The data comes from our partner hospital, the Beth Israel Deaconess Medical Center (BIDMC), and is covered under a prior IRB with the PI of the MIMIC II project, Prof. Roger Mark at MIT.

The latest release of the MIMIC II database contains clinical information for 32,536 subjects, and 23,180 bedside monitoring records (from approximately 13,500 subjects). Of these records, 4,897 waveform records and 5,266 trend records have been matched and time-aligned to 2,809 clinical records. The MIMIC II clinical database contains laboratory data, therapeutic intervention profiles such as vasoactive medication drip rates and ventilator settings, nursing progress notes, discharge summaries, radiology reports, provider order entry data, International Classification of Diseases (ICD-9) Codes. The waveform database contains up to eight waveform signals from the bedside monitors (sampled at 125 Hz), all vital-signs trend data (sampled at 1 Hz), and all bedside monitoring alarms. The MIMIC II data-archiving infrastructure is outlined in Figure 4.1.1.

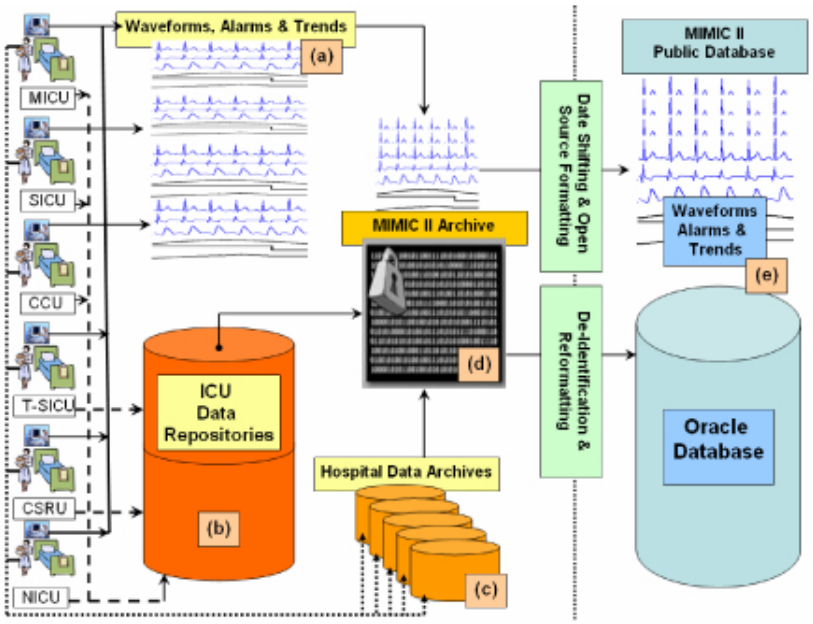

Figure 4.1.1: MIMIC II data-archiving infrastructure at BIDMC. The bedside monitoring data (a) and ICU clinical information (b) are merged with information from the hospital's electronic medical record system (c) to create an archive (d) that contains as many data elements as possible for each ICU patient. The resultant database is de-identified and made available to the interested research community at the MIMIC II database (e).

4.2 Feeding Data to MIMIC II

As the data that we are studying in this project is part of the routine clinical care of the target patient population at BIDMC, it is automatically archived on MIMIC II. The second key step for us was to establish the CNS system as the appropriate hardware interface for archiving the TCD data for transfer to the MIMIC II database. We received clearance from the BIDMC biomedical engineering department for use of the CNS, and the use of the CNS for this purpose has subsequently been approved by an amendment to the MIMIC II IRB, separately from the current project. With the approved IRB to use the MIMIC II database in hand, we were in a position to commence the data-acquisition from the hospital neuro-ICU.

It is important to note that the data-collection infrastructure we have put in place will allow us, through MIMIC II, to collect waveform records beyond the expiration of the current grant, and will thus aid in the development of a research database of significant size and richness.

To date, we have collected and archived ABP, CBFV and ICP waveform data, sampled at 125 Hz, from 26 recording sessions in nine patients. Some of these records have missing signals and have not been analyzed further; the rest are being folded into ongoing analysis, see Chapter 5. The average age of the nine subjects is 59.2 years (with a standard deviation of 15.3 years; range: 48 — 85 years). The GCS scores ranged from 3 to 13 (with a mean of 8 and a standard deviation of 3.7). All patients were in the head-up position, with an average vertical distance of 20.3 cm (standard deviation of 6.5 cm) between the ICP transducer and the ABP transducer.

Across the patients, mean ICP ranged from 3.2 mmHg to 12.1 mmHg. Mean ABP ranged from 78.8 mmHg to 136.0 mmHg, and systolic ABP ranged from 113.0 mmHg to 196.4 mmHg. Figure 4.2.1 shows an example of recorded waveform data with good signal quality (left panel) and a segment of recorded data with some sporadic episodes of noise and artifact (right panel).

The data we collected was turned over to the PhysioNet team for merging with the rest of the MIMIC II database and release to the interested research community through the PhysioNet website (http://physionet.org).

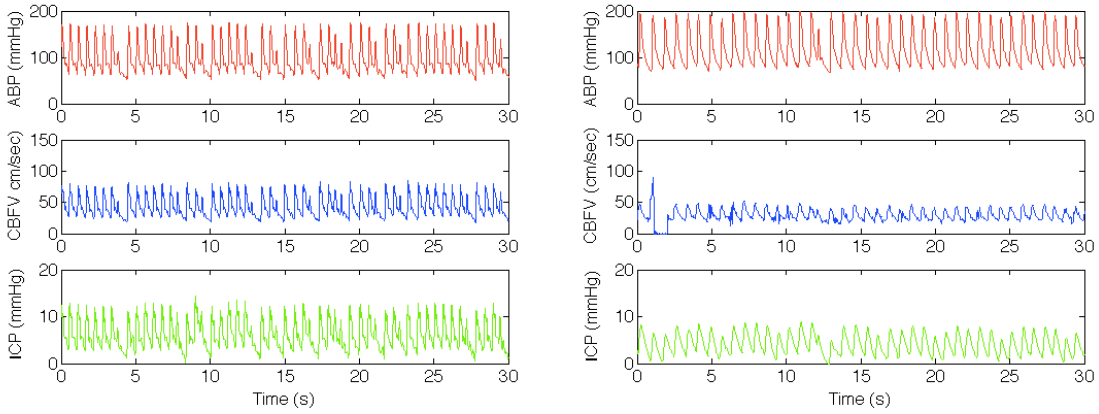

Figure 4.2.1: Examples of acquired data with good signal quality (left panel) and sporadic episodes of noise and artifact (right panel), particularly in the CBFV waveform signal.

Chapter 5

ICP Estimation

We summarize in this chapter our explorations in estimating ICP in patients with subarachnoid hemorrhages. The point of departure for our algorithm refinement and validation is the work described in [1]. We outline the preprocessing steps first, and then compare our estimation results against the invasively measured ICP. We conclude by describing our work in developing a real-time estimation algorithm for ICP.

5.1 Preprocessing

Before ICP can be estimated, the waveforms collected at the bedside must be preprocessed. This important step involves aligning asynchronous waveforms, flagging regions of poor signal quality, and adjusting clinical measurements for patient and sensor positioning.

5.1.1 Coarse time-alignment

The ABP and CBFV signals used to estimate ICP are recorded from separate devices with different processing pathways. The generation of the CBFV waveform requires a series of computations, and the CBFV waveform therefore lags behind the ABP waveform. To align the signals, we first determine the times of the peak values in each cycle of both the ABP and CBFV waveforms, beat-by-beat. We then represent the ABP and CBFV signals as binary sequences with '1' at every index corresponding to the peak of a wavelet and '0' at all other sample times. A coarse alignment

of the ABP and CBFV signals is then obtained by applying the sample offset that maximizes the correlation of the binary sequences. Figure 5.1.1 illustrates this process for an actual patient record.

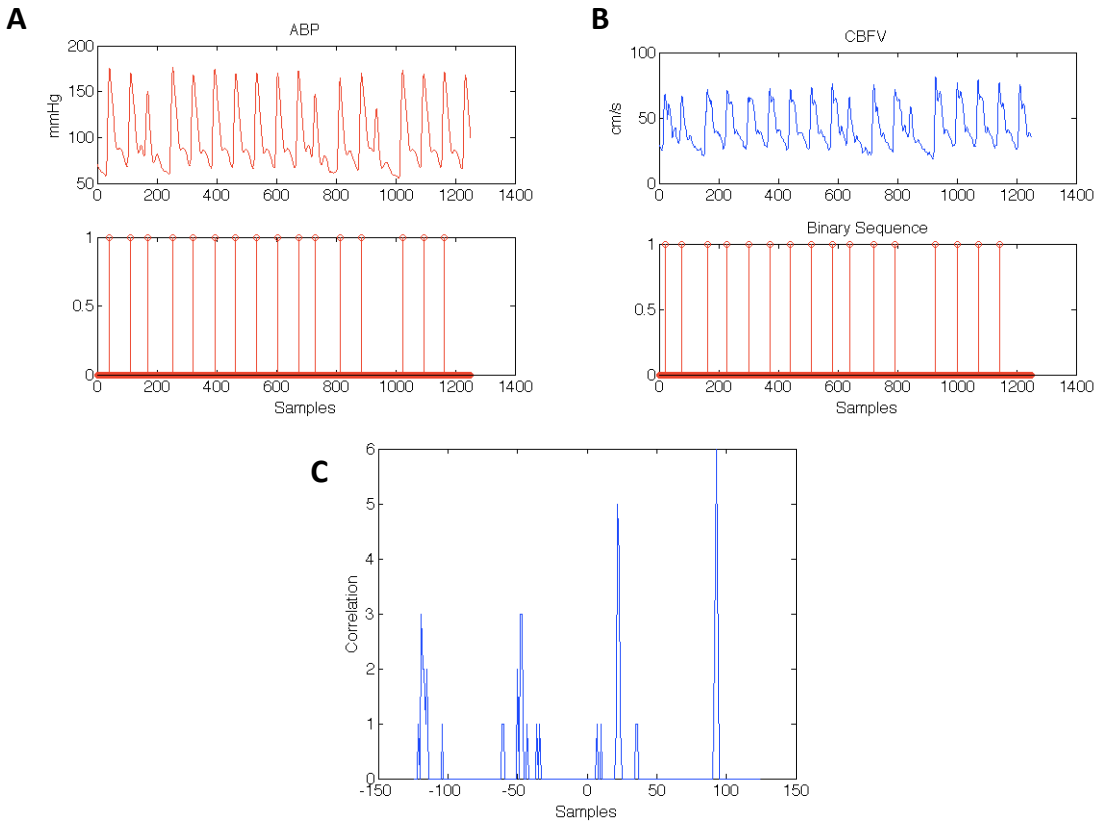

Figure 5.1.1: A, B: An example where we identify the peaks of the ABP and CBFV signals and convert them to binary sequences. C: A plot of the cross-correlation of the binary sequence against the sample offset. In this example, a coarse offset of 93 samples was applied to advance the CBFV signal.

The offsets are restricted to be within 125 samples, or one second, reflecting the latency we expect in our clinical data. In records where our algorithm generates several candidate offsets with the same correlation level, we choose the smallest offset. At the end of this process, we visually inspect the records using fiducial markers, like ectopic beats, to ensure proper alignment; this can eventually be automated.

5.1.2 Signal quality

Once the signals are aligned to within the correct beat, we address the issue of signal quality. In this dataset, the ABP signal is typically relatively low-noise. In contrast, the CBFV waveform often has non-physiological artifacts that are due to the intrinsic difficulty in obtaining a stable CBFV signal with the hand-held TCD transducer probe. Figure 5.1.2 illustrates the varying signal quality of the CBFV waveform.

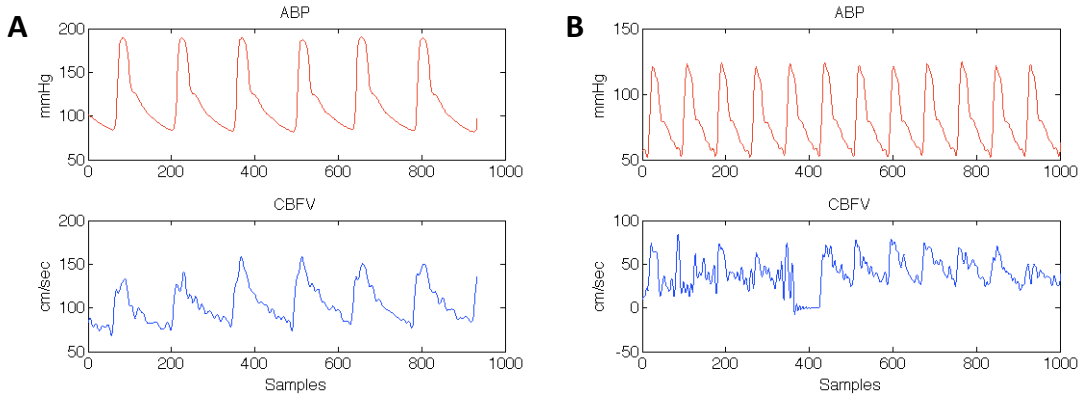

Figure 5.1.2: A: Clean CBFV waveform; B: Distorted and noisy CBFV waveform. In all cases, the ABP waveform is distortion free.

We address this issue by low-pass filtering both the ABP and CBFV signals to eliminate high-frequency noise. We apply a filter with 16 Hz cutoff to the ABP waveform and a filter with a 10 Hz cutoff to the CBFV waveform. We use a lower cutoff frequency to filter the CBFV in order to eliminate the non-physiological artifacts in the beat morphology.

We also flag beats where the CBFV signal is lost. To do so, we first use a beat-onset detection algorithm [6] to identify the beat intervals of the ABP waveform, as this is a cleaner waveform than CBFV. We then reject beats in which the minimum value of the associated CBFV is below a threshold determined by the mean minimum beat-by-beat value across all CBFV beats. Finally, we visually inspect the beats to ensure proper and clean annotations.

5.1.3 Adjusting mean ABP

Patients with brain injury are often positioned with the head-of-bed elevated, so as to relieve possible intracranial congestion. The head-up posture is therefore usually the one in which the recordings of ABP, CBFV, and ICP are being made. The ABP measured in the radial artery and calibrated to heart-level (we denote this pressure by rABP) is consequently higher than the cerebral ABP (cABP), due to the vertical height of the fluid channel connecting these two positions. To produce ICP estimates that are consistent with the invasively measured ICP, we must account for this fluid column between the heart (at which level rABP is measured) and the tragus (at which level ICP is measured and where the arterial blood pressure is cABP). The lack of information about patient and sensor positioning was a major limitation of the TBI data set used for our earlier validation studies, and was a key reason for wanting to set up our own data collection protocol in this project.

We adjust the measured rABP waveform, denoted by $p_r(t)$ in the following equation, by subtracting the pressure due to the fluid column:

$$p_c(t) = p_r(t) - \rho g h \tag{5.1}$$

where $p_c(t)$ is the height-corrected rABP (reflecting cABP), ρ is the density of blood, g is the gravitational acceleration constant, and h is the vertical height between the heart and tragus. Because the density of blood is dependent on the hematocrit, we archive and use the hematocrit value that was reported closest to the time of the TCD examination.

5.2 Estimating ICP

After the waveforms are preprocessed, we estimate ICP using the basic model-based algorithm in [1]. To describe and use the model, an additional small (sub-beat) time-offset is needed. While $p_c(t)$ is obtained from $p_r(t)$ by a height correction, this further time-offset of $p_c(t)$ is required to reflect the different path lengths from heart to the MCA versus heart to the radial artery. Imposing

this sub-beat (or fine) time-offset on $p_c(t)$ results in the waveform $p(t)$:

$$p(t) = p_c(t + \tau) \tag{5.2}$$

where τ is the time-offset. We describe the computation of τ shortly.

Our simplified, aggregated model for the dynamics of the intracranial space can now be written down. It represents the circuit in Figure 2.2.1C, and expresses the CBFV, denoted by $q(t)$, in terms of: $p(t)$; its derivative; the ICP, denoted by p_{ICP} and assumed constant at its mean value over the estimation window; and parameters R and C:

$$q(t) = \frac{p(t) - p_{ICP}}{R} + C\frac{dp(t)}{dt} \ . \tag{5.3}$$

The algorithm in [1] proceeds in stages, first estimating C, then R, then p_{ICP}, at each stage looking for a least-square-error fit of the relevant portion of the model to the measured data over a window comprising several beats. Given the poor signal quality of the CBFV recordings, we look for as large a window of usable ABP and CBFV beats as possible, up to 60 beats, to estimate ICP. Our estimation windows accordingly range from 20 to 60 beats, depending on the data quality in the record under consideration.

5.2.1 Fine time-alignment

We describe here how we choose the fine time-offset used to transform $p_c(t)$ to a cABP waveform $p(t)$ that is better time-aligned to the CBFV. Appropriate and robust selection of this offset remains a challenging task, which we are continuing to investigate.

We estimate the time-offset using an algorithm motivated by the model in Equation 5.3 above. We adjust the time-offset τ that generates $p(t)$ from $p_c(t)$, so as to minimize a mean-square-error criterion in fitting $p(t)$ and $q(t)$ to Equation 5.3. For simplicity, we focus on the vicinity of the extreme points of the ABP waveform, where the derivative term is small, and thus ignore the

compliance term in Equation 5.3. We can then rewrite Equation 5.3 as

$$p(t) \approx Rq(t) + p_{ICP} \tag{5.4}$$

at all the selected points. Candidate time-offsets are applied to five-beat windows of $p_c(t)$ to generate $p(t)$, which is then regressed against $q(t)$ according to Equation 5.4; the time-offset that yields the minimum residual sum of squares for that window is recorded. After all possible windows are considered, the median time-offset is applied to $p_c(t)$ to obtain $p(t)$.

Due to the noise in $q(t)$ and the short data records, we often have to adjust the computed time-offset to produce physiological ICP estimates. When our initial ICP estimates are negative over any region of time, we increment the time-offset, thereby advancing $p(t)$ to be closer in phase to $q(t)$, until the estimates first become positive. (Tightening the phase will tend to reduce the estimated R, which in turn raises the estimated ICP.) When this heuristic has to be invoked, it mainly causes the time-offset to be incremented by 1 or 2 samples.

5.3 Summary of Estimation Procedure

We summarize now the above process for estimating ICP using clinical data from SAH patients:

1. The ABP and CBFV waveforms are coarse-aligned by first locating peaks of both waveforms to create binary sequences with '1' at each peak location and '0' elsewhere. We coarse-align ABP and CBFV by shifting the CBFV signal by an offset that maximizes the correlation between the two binary sequences.

2. The ABP and CBFV waveforms are filtered to remove high-frequency noise. Furthermore, dropped CBFV beats are flagged and removed from further analysis.

3. The mean value of the measured ABP waveform $p_r(t)$ is adjusted to account for the fluid column between the ABP and ICP pressure transducers, thereby resulting in $p_c(t)$.

4. The height-corrected signal $p_c(t)$ is converted to the ABP waveform $p(t)$ in our model by applying a time-offset generated by our time-offset algorithm.

5. We use the algorithm in [1] to estimate ICP for the largest possible window sizes.

5.4 Results and Discussion

We present here the ICP estimates obtained so far, and some preliminary discussion. Our analysis is ongoing, as more data comes in.

We used data collected from 5 patients (4 males, 1 female) with a mean age of 63.6 years. From the 21 patient records used, we obtained 28 non-overlapping windows of data, for each of which we computed an estimate of ICP. The amount of reliable data for each vessel is often very short, reflecting the standard protocol for TCD examinations of SAH patients, with each vessel being insonated for only as long as needed to obtain a reliable flow-velocity signal. We incorporated the maximum number of usable beats per window, up to a maximum of 60 beats. (A smaller maximum would have yielded more windows; this will be explored in later work.)

Our ICP estimates are compared against invasively measured ICP. In Table 5.4.1 below, the rows represents ICP estimates obtained from distinct, non-overlapping windows of data. For each estimate, we include the following information:

- Record Identifier: This includes the patient number, the study number, and the side of the MCA (Left or Right) used to estimate ICP.
- Window Size: The number of ABP and CBFV beats used per window to estimate ICP.
- ICP: The mean value of the invasive ICP measured over the window.
- nICP: The ICP estimate.
- Bias: The bias, defined as nICP$-$ICP, computed for the window.

Across all non-overlapping estimates, the mean bias is -0.7 mmHg, the standard deviation of the error (SDE) is 4.0 mmHg, and the overall root-mean-squared error (RMSE) is 3.9 mmHg. We define the mean bias as the average bias across all non-overlapping ICP estimates, the SDE as the corrected sample standard deviation over the biases, and the RMSE as the square root of the average of the squared non-overlapping biases. The mean bias relates to the accuracy of the method,

Patient #	Study #	Side	Window	ICP	nICP	Bias
7	3	L	30	11.4	12.6	1.2
7	2	R	21	5.2	2.4	−2.8
7	1	R	60	4	3.4	−0.6
7	1	L	60	4.6	2.3	−2.3
5	4	R	60	8.2	1.1	−7.1
5	3	R	60	3.8	0.4	−3.4
5	3	L	60	4.1	13.1	9.0
5	2	R	60	3.7	2.9	−0.8
5	2	R	60	3.8	6.5	2.7
5	2	L	60	4.2	8.3	4.1
3	2	R	60	10.8	3.9	−6.9
3	2	L	30	11.9	3.7	−8.2
3	1	R	30	10.7	7.3	−3.4
3	1	L	60	10.5	5.7	−4.8
3	1	L	60	10.5	13.2	2.7
2	3	R	30	8.4	7.1	−1.3
2	2	R	20	6.9	9.9	3.0
2	2	L	60	7.9	6.6	−1.3
2	1	R	30	7.5	3.5	−4
2	1	L	19	5.7	5.1	−0.6
1	2	L	60	5.9	8.5	2.6
1	2	L	30	5.7	9.7	4.0
1	2	L	30	6.3	2.6	−3.7
1	2	L	60	5.3	4.6	−0.7
1	2	L	30	5.6	5	−0.6
1	2	R	60	5.7	11	5.3
1	2	R	30	6.8	5.4	−1.4
1	1	L	60	5.9	4.9	−1.0

Table 5.4.1: ICP estimates compared with measured ICP.

whereas the SDE relates to the reproducibility of our estimates, or the precision. The RMSE folds both accuracy and precision into a single metric of agreement (and is the root-sum-of-squares of the bias and the uncorrected standard deviation, hence approximately the root-sum-of-squares of the bias and corrected standard deviation). We summarize the results obtained for the SAH population in a Bland-Altman plot, Figure 5.4.1

To complement Table 5.4.1, we include plots (Figures 5.4.2–5.4.6 below) to highlight the performance, both good and bad, of our algorithm. Each figure contains a plot of the continuous invasively-obtained ICP, overlaid with the nICP estimate of the mean value of ICP in that win-

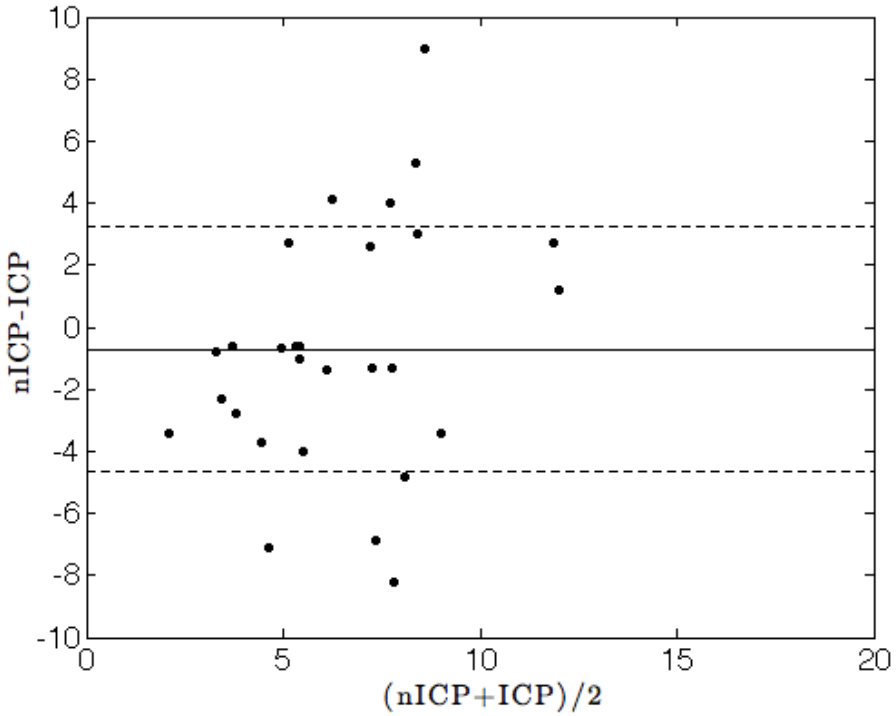

Figure 5.4.1: Bland-Altman plot of ICP estimates.

dow. The last example (Figure 5.4.6) shows the estimates from two non-overlapping windows, and conveys a sense of the rate at which we generate new estimates.

5.4.1 Discussion and Extensions

Improvements over previous validation results The results in Table 5.4.1 represent a substantial performance improvement over the ICP estimates obtained using unilateral CBFV recordings on TBI patients in our earlier work, [1]. The mean bias, SDE, and RMSE of the SAH ICP estimates are all reduced by nearly a factor of 2 when compared to the TBI ICP estimates in [1].

Sub-analysis of left and right MCAs Table 5.4.1 contains the results obtained from analyzing the CBFV signals from the right and the left MCA. If we compute the mean bias, SDE, and RMSE separately for the nICP estimates obtained from the right and the left side of the brain, we obtain a mean bias of -1.6 mmHg, an SDE of 3.7 mmHg, and an RMSE of 3.9 mmHg for the right side, and 0.03 mmHg, 4.2 mmHg, and 4.0 mmHg, respectively, for the left side of the brain. This sub-analysis

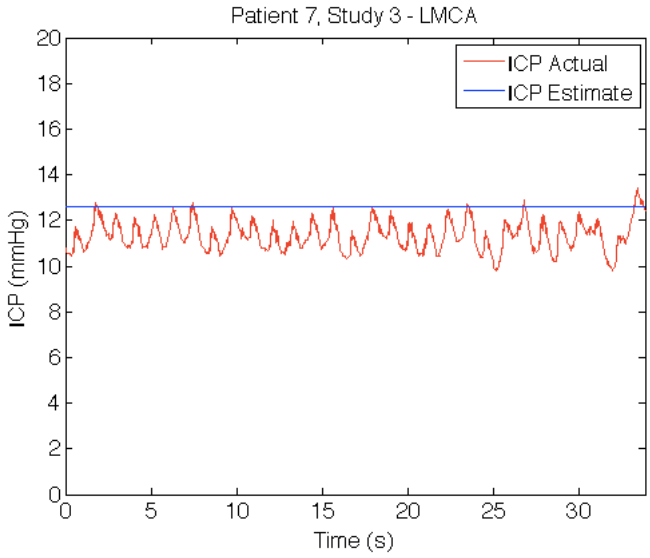

Figure 5.4.2: The estimate exceeds the actual mean ICP, but not by much.

demonstrates that our estimation approach robustly estimates ICP from either MCA. Furthermore, it also demonstrates that the overall mean bias is not accidentally low by averaging high values of the bias (but of opposing signs) obtained from estimating ICP from either hemisphere.

Other vessels In the results above and in all our prior validation work, we estimated ICP using measurements from the MCA. Here, we report our explorations in estimating ICP using other arteries in the brain. We provide examples of the waveforms from the different vessels (Figures 5.4.7-5.4.9) and estimate ICP using windows that range from 5 beats to 45 beats. Out of the vessels examined, we are able to obtain estimates that are comparable to or even better than those obtained by using the MCA. We summarize our results in Table 5.4.2.

Patient. #	Study #	Vessel	Window	ICP	nICP	Bias
7	3	Left internal carotid	45	11.6	10.2	−1.4
7	2	Left posterior cerebral	5	6.8	7.8	1.0
5	4	Left vertebral	30	7.1	2.2	−4.9

Table 5.4.2: ICP estimates using vessels other than the right or left MCA.

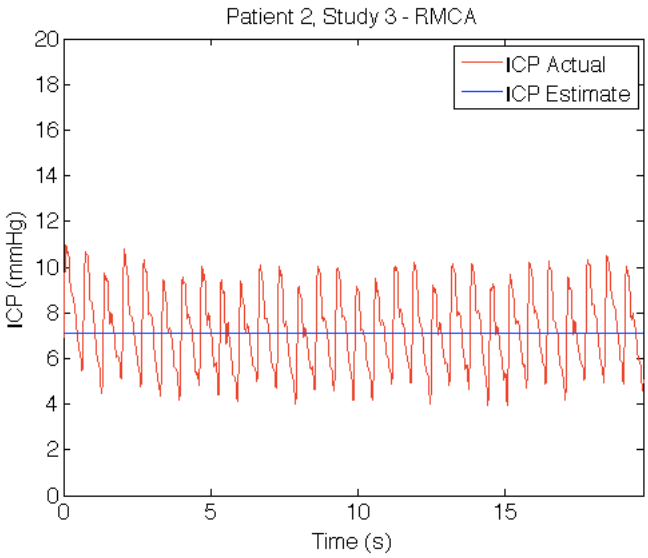

Figure 5.4.3: The estimate lies below the actual mean ICP, but not much below.

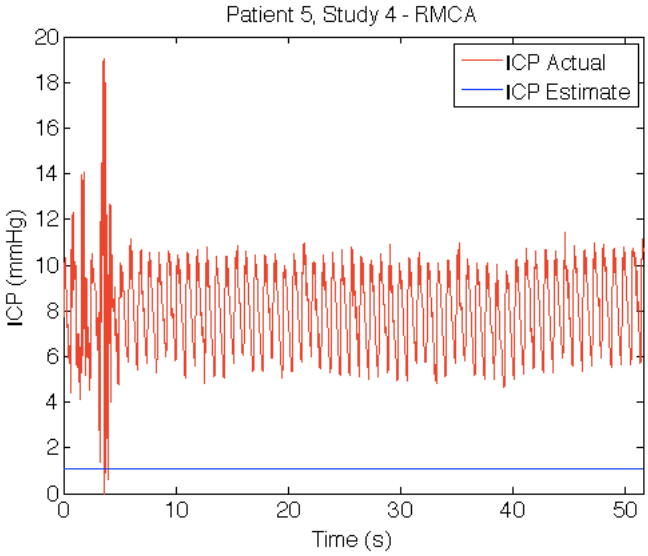

Figure 5.4.4: The estimate lies well below the mean ICP for this window.

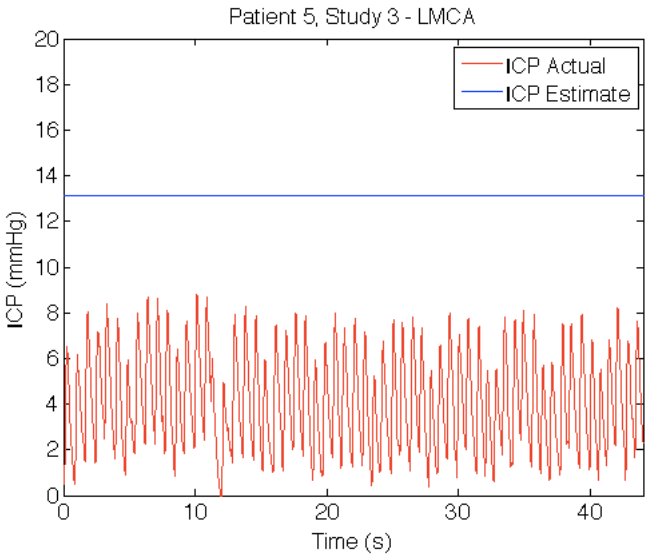

Figure 5.4.5: The estimate lies well above the mean ICP for this window.

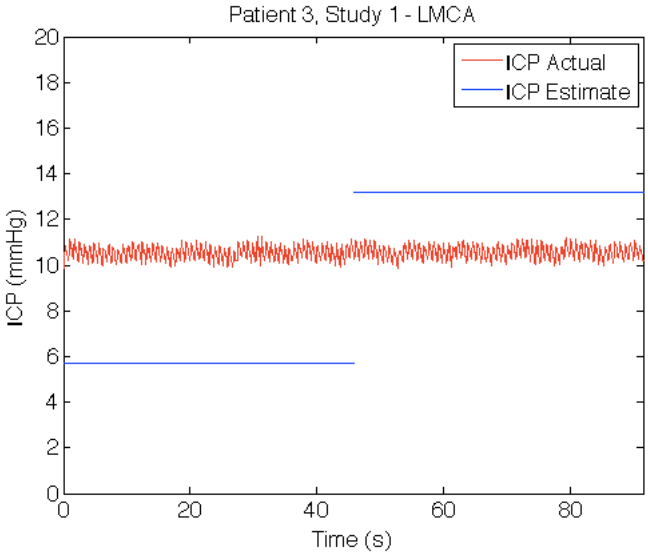

Figure 5.4.6: Estimates of ICP from two non-overlapping windows.

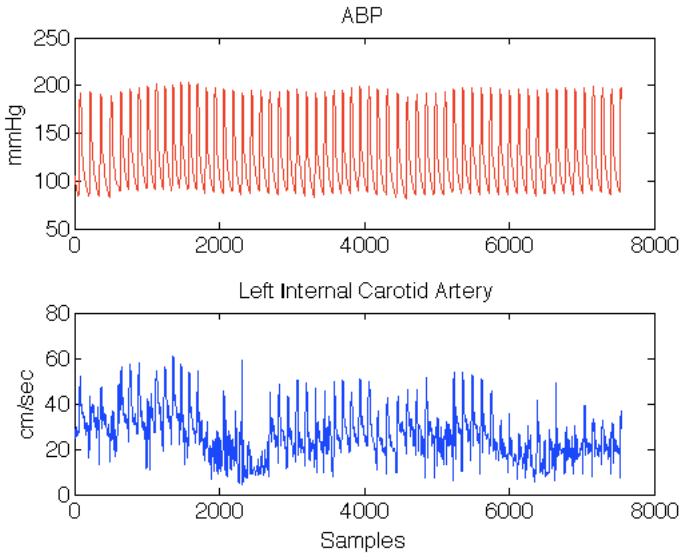

Figure 5.4.7: Patient 7, Study 3, left internal carotid artery.

5.4.2 Performance benchmark

We now take a critical look at our preliminary results.

Compared to the TBI patients in [1], the SAH patients in neurocritical care tend to have low and relatively constant ICP. Of the 28 non-overlapping windows, the mean of the invasively measured ICP is 6.8 mmHg with a standard deviation of 2.5 mmHg (range: 3.8 to 11.9 mmHg). This motivates the comparison of our algorithm's performance against a strawman competing "algorithm" that always estimates a predetermined constant ICP for all records and all patients.

For the data that we actually used for ICP estimation, the best constant ICP estimate in terms of mean-square error is the mean ICP over all the non-overlapping windows, which we denote here by y; as noted above, $y = 6.8$ mmHg. Therefore, our algorithm would outperform y in terms of the mean-squared-error if the following holds:

$$\frac{1}{N}\sum_{n=1}^{N}(x_n - \hat{x}_n)^2 < \frac{1}{N}\sum_{n=1}^{N}(x_n - y)^2 = \sigma^2 \tag{5.5}$$

where x_n is the mean ICP for the n^{th} non-overlapping window, $\hat{x}_n$ is the ICP estimate for the n^{th} non-overlapping window, and σ^2 is the variance of all the x_i's. For a comparison of RMSE's, simply

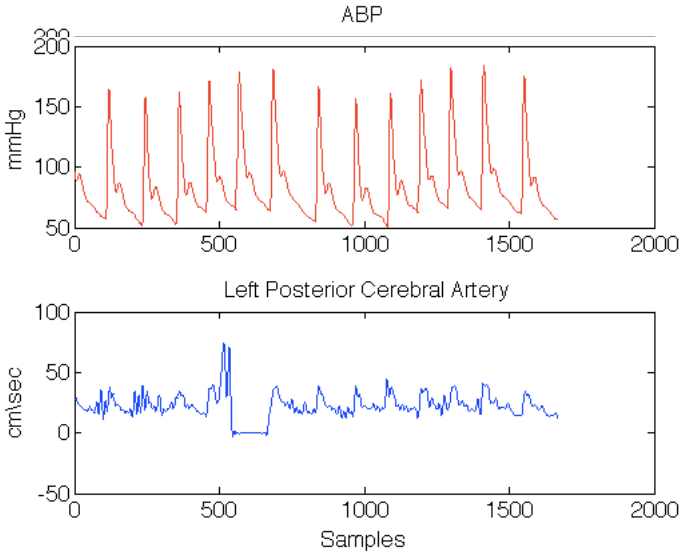

Figure 5.4.8: Patient 7, Study 2, left posterior cerebral artery.

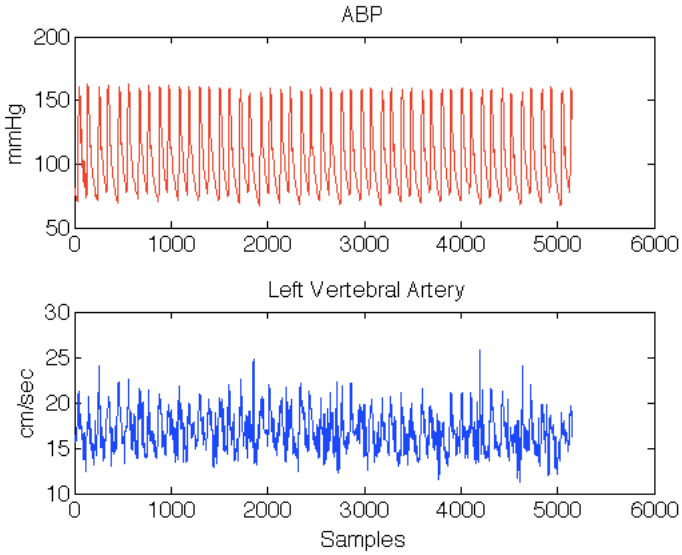

Figure 5.4.9: Patient 4, Study 4, left vertebral artery.

take the square root of each side.

Unfortunately, since our RMSE is 3.9 mmHg over the 28 windows, while the standard deviation of the mean ICP over these windows is 2.5 mmHg, the relationship above shows that a constant ICP estimate of 6.8 mmHg outperforms our algorithm in terms of (root) mean-squared error.

Given that the competing algorithm will not know y in advance, we consider how the two algorithms will compare if the competing estimate is $y + c$, where c is the departure from the true mean ICP. Using a similar argument, we will outperform the constant estimator in terms of mean-squared error when

$$\frac{1}{N}\sum_{n=1}^{N}(x_n - \hat{x}_n)^2 < \sigma^2 + c^2 \tag{5.6}$$

Using the results summarized in Table 5.4.1, we outperform the constant estimator only when the deviation c away from the mean that it picks has magnitude larger than around 3 mmHg. Given that the measured average ICP over the 28 windows has a standard deviation of 2.5 mmHg, the standard error of the mean is $2.5/\sqrt{28}$ which is around 0.5 mmHg, so it is unlikely that the competing algorithm would pick a constant estimate that was as far away as 3 mmHg from the mean.

Though the above comparison may seem unfavorable to our algorithm, the following two facts should be kept in mind. First, our algorithm — essentially in the form used in the present study — has also performed well in tracking ICP's in TBI patients that varies dynamically over a range of 100 mmHg, as shown in [1]. The strawman competing algorithm presented here would be severely out of luck in that domain. Second, our results here have shown an improvement by a factor of around 2 relative to the performance metrics in our previous TBI validation. This gives reason to expect that the same care in data collection and analysis will translate to greatly improved performance in the TBI setting and beyond.

5.5 Real-time ICP estimation

We have developed a version of our ICP estimation algorithm that runs in real-time on continuously streamed data from component devices, such as the Spencer TCD or a Finapres noninvasive

arterial blood pressure monitor. For this purpose, we have developed the signal pipeline that is schematically described in Figure 5.5.1. To acquire the ABP and CBFV data, we use a National Instruments DAQ-mx analog-to-digital (A/D) conversion card with a sampling rate of up to 10,000 samples/second, though operated nominally at 200 samples/second. This particular A/D card is USB enabled and can thus be connected to laptop or desktop computers. For our prototyping purposes, we used the Matlab Data Acquisition Toolbox to control the data-acquisition step. Likewise, the signal-conditioning step and the ICP estimation algorithm are also implemented in the Matlab scientific computing environment.

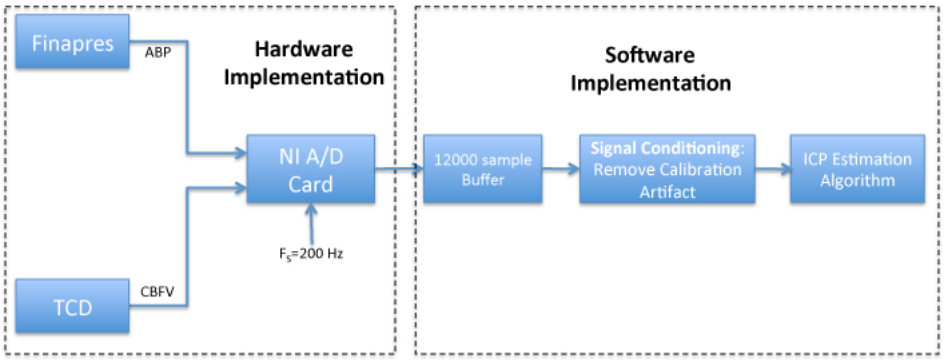

Figure 5.5.1: Signal processing steps for real-time ICP estimation.

We have tested the A/D front-end by streaming CBFV data from our ST3 TCD system and ABP data from a Finapres noninvasive ABP monitoring system (Figure 5.5.2). We have also

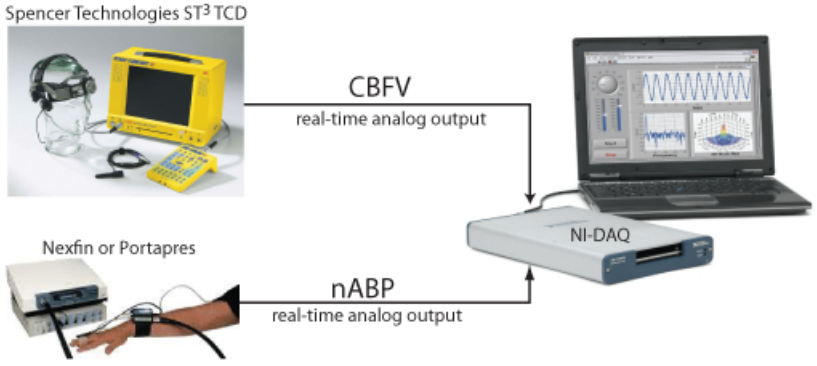

Figure 5.5.2: Data collection set-up for real-time ICP estimation from cerebral blood flow velocity and noninvasive arterial blood pressure waveform measurements.

converted the estimation algorithm to run in real-time on data buffers of 60 seconds. Segments of ABP and CBFV data are stored in the front-end data buffer. Once the buffer is filled, the signal-conditioning algorithms are applied, and the ICP estimation algorithm is called to produce one estimate of mean ICP for each data window. Since the calculations required for the signal conditioning and ICP estimation are computationally inexpensive, the signal conditioning and ICP estimation steps execute before then next 60-second buffer is filled with data. The ICP estimation is therefore performed in real-time, only encountering a delay associated with the filling up of the buffer. This delay is not significant in clinical applications.

We have also developed a GUI-based tool for annotation correction, which can be incorporated into a real-time system for retrospective analysis of annotation quality, see Figure 5.5.3. In addition, we developed a Matlab-based GUI for the real-time ICP estimation system, with options of changing filter parameters interactively and while the estimation routine is running, see Figure 5.5.4.

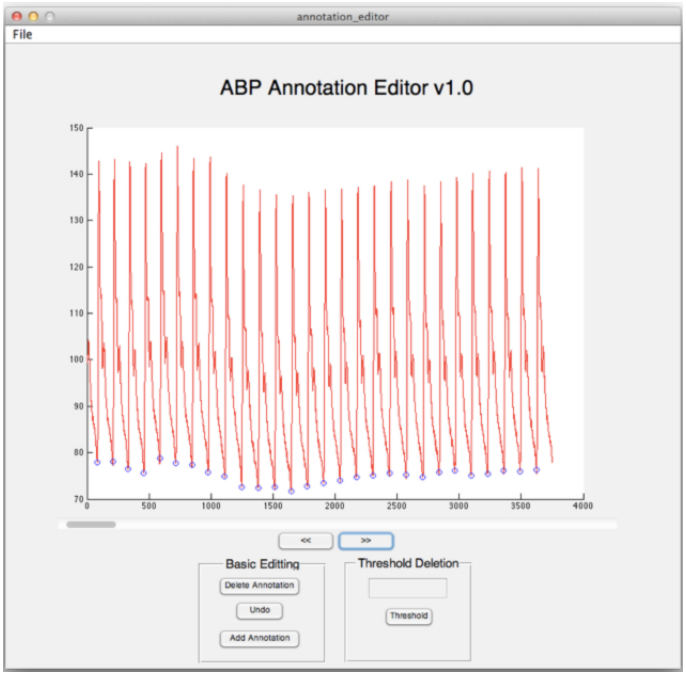

Figure 5.5.3: Graphical User Interface for retrospective analysis of waveform annotation process. Shown are the beat-onset annotations for the arterial blood pressure (ABP) waveform.

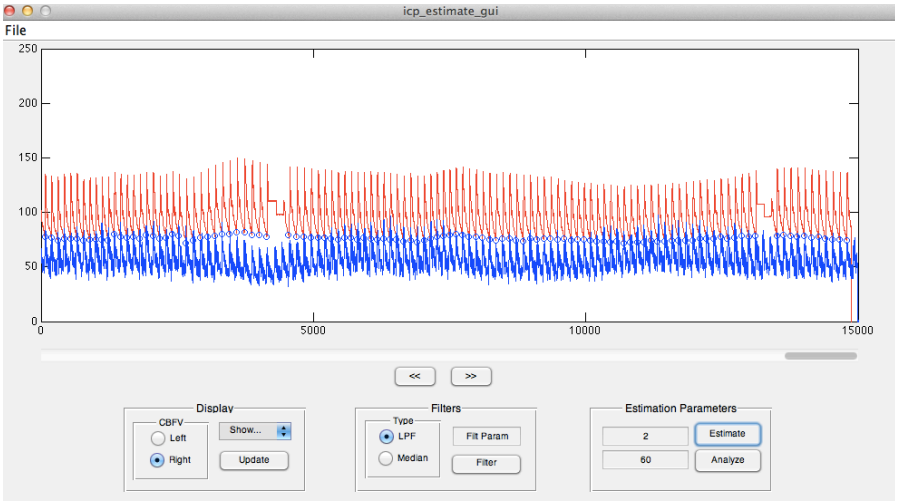

Figure 5.5.4: Graphical User Interface for real-time ICP estimation, where estimation parameters can be dynamically updated.

Acknowledgements We are very grateful to Prof. Roger Mark of MIT for help getting us connected to MIMIC II, and to our clinical collaborators at Boston's Beth Israel Deaconess Medical Center (BIDMC) — Drs. Ajith Thomas, D. Eric Searls, Vasileios Lioutas, and Shruti Sonni — for organizing and carefully implementing the data collection. Drs. Vera Novak and Magdy Selim of BIDMC were also helpful at the initiation of the project.

Chapter 6

Key Research Results

- We have developed and deployed a data-acquisition infrastructure for collecting high-resolution waveform data from patients with critical injuries to their brain. We will continue to leverage this infrastructure to collect data for noninvasive estimation of ICP, even past the end of the present project.
- We have developed the first public-access database of ABP, CBFV, and ICP for testing of algorithms for noninvasive ICP estimation. The database will continue to grow.
- We have improved upon our previous results of model-based, patient-specific, calibration-free, continuous, and noninvasive estimation of ICP. Specifically, we were able to increase both the accuracy (reducing the mean bias) and the precision (reducing the standard deviation of the error) of our ICP estimates by a factor of two, compared to our previous results on archived data from TBI patients.
- We demonstrated that our noninvasive ICP estimates can be obtained from either right or left MCA with the same high accuracy and precision. Furthermore, we were able to demonstrate that the accuracy and precision of ICP estimation remains comparable if the CBFV signal from cerebral vessels other than the MCA is used. These results have significant implications for further development of this technology.
- We have demonstrated real-time operation of our noninvasive ICP estimation algorithm.

Chapter 7

Reportable Outcomes

Below, we list the reportable outcomes of the research funded through this award.

Abstracts

- I Hwang, FM Kashif, GC Verghese, T Heldt. A frequency-domain approach to model-based noninvasive intracranial pressure estimation from arterial blood pressure and cerebral blood flow velocity. Invited contribution to the Minisymposium on Information Derived from the Arterial Blood Pressure Waveform and Its Significance. IEEE Engineering in Medicine and Biology Conference, San Diego, CA, September 2012.

- T Heldt, GC Verghese. Modeling the morphology of the intracranial pressure waveform. Invited contribution to the Minisymposium on Computational Modeling for Scientific Inquiry. IEEE Engineering in Medicine and Biology Conference, Osaka, Japan. July 2013.

- J Noraky, GC Verghese, DE Searls, V Lioutas, S Sonni, A Thomas, T Heldt. Noninvasive intracranial pressure estimation in patients with subarachnoid hemorrhage. Submitted to the 2013 Intracranial Pressure Conference, Singapore.

Presentations

- T Heldt, GC Verghese. Model-based noninvasive estimation of intracranial pressure. Joint Grand Rounds presentation to the U.S. Army Medical Research and Materiel Command and

U.S. Army Telemedicine and Advanced Technology Research Center, Ft. Detrick, MD, July 2012. (Presenter: T Heldt)

- I Hwang, FM Kashif, GC Verghese, T Heldt. A frequency-domain approach to model-based noninvasive intracranial pressure estimation from arterial blood pressure and cerebral blood flow velocity. Mini-symposium on Information Derived from the Arterial Blood Pressure Waveform and Its Significance. IEEE Engineering in Medicine and Biology Conference, San Diego, CA, September 2012. (Presenter: T Heldt)

- T Heldt, GC Verghese. Model-based neuromonitoring. University of Maryland Shock Trauma Center, Baltimore, MD, September 2012. (Presenter: T Heldt)

- FM Kashif, GC Verghese, T Heldt. Model-based noninvasive estimation of intracranial pressure. Medical Electronics Workshop, National Taiwan University, Taipei, Taiwan, November 2012. (Presenter: T Heldt)

- T Heldt, GC Verghese. Challenges (and some solutions) in patient monitoring. Samsung Advanced Institute of Technology, Yongin, South Korea, December 2012. (Presenter: T Heldt)

- T Heldt. Noninvasive intracranial pressure monitoring. Fiction or reality? Boston University/Boston Medical Center Joint Neurology-Neurosurgery Grand Rounds, Boston, MA, January 2013.

- T Heldt. Neurocritical Care Informatics: Leveraging data and models to understand the physiology of the injured brain. Department of Electrical Engineering and Computer Science and Institute for Medical Engineering and Science, Massachusetts Institute of Technology, Cambridge, MA. April 10, 2013.

- T Heldt. Neurocritical Care Informatics: Leveraging data and models to understand the physiology of the injured brain. Department of Biomedical Engineering, University of Illinois at Chicago, Chicago, IL. May, 2013.

- GC Verghese. Computational systems physiology at the bedside. Institute for Computational Medicine, Johns Hopkins University, Baltimore, MD, May 2013.

- T Heldt. Modeling, Model Identification, and Model Reduction in Biomedicine. Invited keynote lecture. IV Congress of Applied, Computational and Industrial Mathematics, Society for Industrial and Applied Mathematics (SIAM), Buenos Aires, Argentina, May, 2013.

- T Heldt, GC Verghese. Modeling the morphology of the intracranial pressure waveform. IEEE Engineering in Medicine and Biology Conference, Osaka, Japan. July 2013. (Presenter: T Heldt)

Degrees obtained

- Irena Hwang, MEng, Department of Electrical Engineering and Computer Science, Massachusetts Institute of Technology, June 2012.

- James Noraky, SB, Department of Electrical Engineering and Computer Science, Massachusetts Institute of Technology, June 2013.

Database The data collected from neurocritical care patients under this project augment the Multiparameter Intelligent Monitoring in Intensive Care II (MIMIC II) database and have been released to PhysioNet (http://physionet.org) for release to the interested research community. To date, 26 patient records from nine patients have been released, though the database will continue to grow as we will continue to collect data in collaboration with our clinical colleagues and update the database periodically.

Funding opportunities pursued

- T Heldt (PI), Noninvasive intracranial pressure monitoring in pediatric patients. NIH R21 Exploratory/Developmental Research Grant Award, National Institute of Neurological Disorders and Stroke (NINDS).

- T Heldt (PI), Computational models of fluid redistribution to understand spaceflight-induced intracranial hypertension and visual impairment. National Aeronautics and Space Administration (NASA).

- GC Verghese (PI), Noninvasive intracranial pressure monitoring for spaceflight applications. National Space Biomedical Research Institute (NSBRI).

Employment or research opportunities applied for and/or received

- FM Kashif, Postdoctoral Associate, took job as Senior Research Engineer, Masimo Corporation, Irvine, CA. April 2012.

- G Verghese, Professor of Electrical Engineering, was named Henry Ellis Warren Professor and Professor of Electrical and Biomedical Engineering, Department of Electrical Engineering and Computer Science, MIT. February 2012.

- I Hwang, graduate research assistant, was admitted to Stanford University's doctoral program in Electrical Engineering. April 2012.

- T Heldt, Research Scientist, was promoted to Principal Research Scientist with the Research Laboratory of Electronics, MIT. July 2012.

- J Noraky, undergraduate research assistant, was admitted to MITs doctoral program in Electrical Engineering and Computer Science. April 2013.

- T Heldt, Principal Research Scientist, was appointed Assistant Professor of Electrical and Biomedical Engineering, Department of Electrical Engineering and Computer Science, and Hermann von Helmholtz Career Development Professor with the Institute for Medical Engineering and Science, MIT. July 2013.

Chapter 8

Conclusions

This project has significantly advanced our understanding of the potential and strength of our approach to noninvasive estimation of ICP, and has helped to delineate the next set of challenges. It has also launched a valuable neuro-ICU data collection effort that will extend past this project and continue to expand a database that is accessible to researchers worldwide.

The method has held up well on a very different study population, namely SAH patients, than used in our initial validation studies, which were on TBI patients. Given that ICP in these SAH patients is mostly controlled to low levels, it was not obvious that the model used in our earlier studies would suffice to support estimation in SAH patients. That model was predicated on ICP being sufficiently higher than venous pressure to induce venous collapse. Without this, it is not evident that sufficient information exists to estimate ICP from ABP and CBFV.

The major improvement in our estimation metrics (bias, standard deviation of error, and root-mean-square error) relative to our earlier validation studies in TBI patients comes in part from the more careful data collection, with attention to such issues as patient and sensor positioning, and with better instrumentation than in previous work. On the other hand, a major challenge has been to work with data collected in the course of routine TCD evaluation of SAH patients. The individual records are generally much shorter than in our earlier validation database. This has presented new challenges, for fine time-offset determination as well as ICP estimation, particularly in the face of dropped CBFV beats. We anticipate further development on these fronts, as we move towards robust, stand-alone real-time estimation.

An attractive feature of the data collected under this project is that CBFV is recorded at several major cerebral arteries. This has allowed us to verify — in a preliminary way, but more extensive testing is planned — that ICP can be reliably estimated from any cerebral artery that yields a good CBFV waveform, not only from the MCA. This was a prediction of our model, and it has been gratifying to see it hold up.

Bibliography

[1] FM Kashif, GC Verghese, M Czosnyka, V Novak, T Heldt. Model-based noninvasive estimation of intracranial pressure from cerebral blood flow velocity and arterial blood pressure. Science Translational Medicine 4(129): 129ra44, 2012.

[2] FM Kashif, T Heldt, GC Verghese. Model-based estimation of intracranial pressure and cerebrovascular autoregulation. Computers in Cardiology 35:369-371, 2008.

[3] FM Kashif. Modeling and estimation for noninvasive monitoring of intracranial pressure and cerebrovascular autoregulation. PhD Thesis, Department of Electrical Engineering and Computer Science, Massachusetts Institute of Technology, Cambridge, MA, 2011.

[4] M Ursino, CA Lodi. A simple mathematical model of the interaction of intracranial pressure and cerebral hemodynamics. Journal of Applied Physiology 82(4):1256-1269, 1997.

[5] M Saeed, M Villarroel, AT Reisner, G Clifford, LW Lehman, G Moody, T Heldt, TH Kyaw, B Moody, RG Mark. Multiparameter Intelligent Monitoring in Intensive Care II: a public-access intensive care unit database. Critical Care Medicine 39(5):952-960, 2011.

[6] W Zong, T Heldt, RG Mark. An open-source algorithm to detect the onset of arterial blood pressure pulses. Computers in Cardiology 30:259-262, 2003.

[7] IT Hwang. Frequency-domain model-based intracranial pressure estimation. Master of Engineering thesis, Department of Electrical Engineering and Computer Science, Massachusetts Institute of Technology, Cambridge, MA, 2012.